

Eagle-Vision-Based Object Detection Method for UAV Formation in Hazy Weather

LI Hao, DENG Yimin*, XU Xiaobin, SUN Yongbin, WEI Chen

School of Automation Science and Electrical Engineering, Beihang University, Beijing 100083, P.R. China

(Received 18 May 2020; revised 30 June 2020; accepted 25 July 2020)

Abstract: Inspired by eagle's visual system, an eagle-vision-based object detection method for unmanned aerial vehicle (UAV) formation in hazy weather is proposed in this paper. To restore the hazy image, the values of atmospheric light and transmission are estimated on the basis of the signal processing mechanism of ON and OFF channels in eagle's retina. Local features of the dehazed image are calculated according to the color antagonism mechanism and contrast sensitivity function of eagle's visual system. A center-surround operation is performed to simulate the response of reception field. The final saliency map is generated by the Random Forest algorithm. Experimental results verify that the proposed method is capable to detect UAVs in hazy image and has superior performance over traditional methods.

Key words: object detection; eagle visual system; UAV formation; image dehazing

CLC number: TP273

Document code: A

Article ID: 1005-1120(2020)04-0517-11

0 Introduction

Locating and collision avoidance are the essential tasks in the formation maintenance and reconstruction. Unmanned aerial vehicle (UAV) detection provides guarantees for solving these tasks, thus enhances the anti-interference ability and robustness of formation in challenging environments. Object detection has been widely studied in recent years. Its implementations can be mainly divided into three classes: pixel-based analysis methods, feature-based methods^[1] and deep learning methods^[2]. Pixel-based methods such as inter-frame difference algorithm and optical flow are efficient, but only capable of moving target detection. Feature-based methods, commonly include image matching, saliency detection and feature classifier, are less robust in complex environments. With the development of computer vision technology, object detection method based on deep learning has greatly improved the accuracy of detection tasks. However, deep learning methods have high computational

complexity, which makes it difficult to be implemented on a UAV platform with limited memory. Compared with general object detection task, object detection of UAV faces the following technical challenges: (1) The environment is often affected by adverse lighting or weather conditions such as haze and rain, and (2) the scale of object changes drastically, hence it is easy to miss small targets. It is imperative to ensure the detectors work reliably in the presence of such conditions. Although current object detection methods can obtain remarkable results on benchmark dataset, they have limited abilities in applying to adverse conditions such as hazy weather.

Biological vision-based approach provides innovative ideas for solving computer vision tasks. It is widely known that eagles have superb vision. The high spatial acuity and contrast sensitivity of eagle eye enable eagles to spot targets accurately during hunting. Currently, the raptor's vision mechanisms have employed for contour detection^[3], saliency detection^[4], aerial refueling^[5-6], autonomous landing^[7], target detection^[8], imaging guidance^[9], etc.

*Corresponding author, E-mail address: ymdeng@buaa.edu.cn.

How to cite this article: LI Hao, DENG Yimin, XU Xiaobin, et al. Eagle-vision-based object detection method for UAV formation in hazy weather[J]. Transactions of Nanjing University of Aeronautics and Astronautics, 2020, 37(4): 517-527.

<http://dx.doi.org/10.16356/j.1005-1120.2020.04.003>

Inspired by eagle vision mechanism, an object detection method for UAV formation in hazy weather is proposed in this paper. The main contributions of this paper are: (1) An image dehazing method is proposed in this paper. Based on the structure and interactions of eagle's retina, the ON and OFF channels are modeled to estimate the atmospheric light and transmission of hazy image. (2) An object detection method is proposed based on the eagle's visual attention mechanism. Color antagonism and the contrast sensitivity function of eagle eye are introduced for feature extraction. Compared with traditional methods, the proposed method can restore the details and features of hazy image more naturally, and shows advantages in accuracy and reliability of UAV object detection.

The rest of this paper is organized as follows. Section 1 presents an image dehazing method based on the ON and OFF channels. In Section 2, a visual attention model of eagle is established for object detection. Comparative experiments are conducted and simulation results are shown in Section 3. Conclusions are given in Section 4.

1 Eagle-Vision-Based Dehazing

A number of traditional state-of-the-art dehazing algorithms^[10-11] have obvious halo effects and color shift in large sky regions, which makes it unsuited for UAV image dehazing. To overcome these drawbacks, an eagle-vision-based dehazing method is proposed.

1.1 ON and OFF channels

In biological visual system, fovea is the most acute and crucial area in retina. Different from mammals with one single fovea, eagle has a deep fovea in the middle of the retina and a shallow fovea in the temporal retina, which is considered to be an important factor for their outstanding vision^[12].

Eagle's retina is mainly composed of several types of nerve cells: Photoreceptors, horizontal cells, bipolar cells, amacrine cells and ganglion cells. Cones and rods, two types of photoreceptors in eagle's retina, dominate bright and scotopic vision respectively. The photoreceptors hyperpolarize to light and release neurotransmitter glutamate on bipolar cells. Bipolar cells are divided into two types based on the different acts on the neurotransmitter: ON bipolar cell that produces a depolarization and OFF bipolar cell that produces a hyperpolarization. The photoreceptors make synapses with ON bipolar cells and OFF bipolar cells, and two types of bipolar cells make synapses with ON and OFF ganglion cells respectively. These cells with their electrical synapses together form a pathway in retina that is ON and OFF channels^[13]. Cones and rods transmit electric signals differently in the ON and OFF channels. Concretely, cones transmit signals to ON and OFF cone bipolar cells and subsequently to ganglion cells. Different from cones, rod bipolar cells do not transmit signals to ganglion cells directly, but make synapses with AII type amacrine cells instead. The rod signals are then relayed to ON and OFF cone bipolar cells by amacrine cells, carrying the signals to ganglion cells in the retina. Moreover, horizontal cells also have a certain adjustment effect on the signals. The interaction between various cells completes the transmission and perception of lightness and darkness in retina, simplified as shown in Fig.1, where HC, BC, AC and GC are short for horizontal cell, bipolar cell, amacrine cell and ganglion cell, respectively, and “+” and “-” denote ON-type and OFF-type cells.

ize to light and release neurotransmitter glutamate on bipolar cells. Bipolar cells are divided into two types based on the different acts on the neurotransmitter: ON bipolar cell that produces a depolarization and OFF bipolar cell that produces a hyperpolarization. The photoreceptors make synapses with ON bipolar cells and OFF bipolar cells, and two types of bipolar cells make synapses with ON and OFF ganglion cells respectively. These cells with their electrical synapses together form a pathway in retina that is ON and OFF channels^[13]. Cones and rods transmit electric signals differently in the ON and OFF channels. Concretely, cones transmit signals to ON and OFF cone bipolar cells and subsequently to ganglion cells. Different from cones, rod bipolar cells do not transmit signals to ganglion cells directly, but make synapses with AII type amacrine cells instead. The rod signals are then relayed to ON and OFF cone bipolar cells by amacrine cells, carrying the signals to ganglion cells in the retina. Moreover, horizontal cells also have a certain adjustment effect on the signals. The interaction between various cells completes the transmission and perception of lightness and darkness in retina, simplified as shown in Fig.1, where HC, BC, AC and GC are short for horizontal cell, bipolar cell, amacrine cell and ganglion cell, respectively, and “+” and “-” denote ON-type and OFF-type cells.

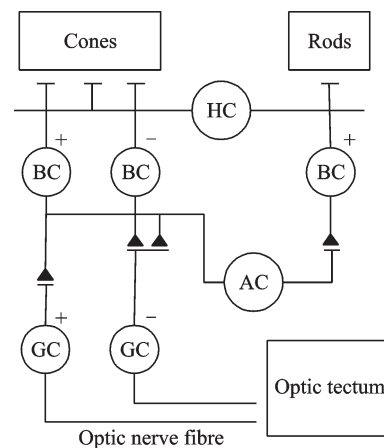


Fig.1 A simplified schematic of ON and OFF channels

In eagle's visual system, the ON channels perceive lightness while the OFF channels perceive darkness. For a hazy image $I^c(x, y)$, we normalize

each color channel, the input signals transmitted by photoreceptors are computed as follows

$$I_{pr}^{on}(x,y) = \max_{c \in \{R,G,B\}} I^c(x,y) \quad (1)$$

$$I_{pr}^{off}(x,y) = \min_{c \in \{R,G,B\}} I^c(x,y) \quad (2)$$

where $I_{pr}^{on}(x,y)$ and $I_{pr}^{off}(x,y)$ refer to the input signals of ON and OFF channels respectively, and R , G , B represent red, green and blue channels of the image.

1.1.1 Horizontal cells

Lateral connected horizontal cells receive a wide range of output signals transmitted by photoreceptors, integrate and modulate the signals according to the brightness. A triphasic modulation of horizontal cells is thought to enhance contrast of images^[14]. Thus, we use a modified sigmoid function $s(p)$ to simulate the effect of modulation. The outputs of horizontal in ON and OFF channels are defined as follows

$$I_{HC}^{\delta}(x,y) = s(I_{pr}^{\delta}(x,y)) \quad (3)$$

$$s(p) = 1 / \{1 + \exp[-(\alpha p + \beta)]\} \quad p \in [0, 1] \quad (4)$$

where $\delta \in \{on, off\}$, α and β are constant parameters which control the shape and translation of $s(p)$, respectively.

1.1.2 Bipolar cells

Bipolar cells have receptive fields with a center-surround structure, which helps to transmit high-accuracy visual information. A Gaussian function is used to simulate the response of receptive field. The output of ON and OFF bipolar cells $I_{BC}^{\delta}(x,y)$ are computed as follows

$$I_{BC}^{\delta}(x,y) = I_{HC}^{\delta}(x,y) \times G(x,y; \sigma_{BC}) \quad (5)$$

$$G(x,y; \sigma) = \frac{1}{2\pi\sigma^2} \exp\left(-\frac{x^2 + y^2}{2\sigma^2}\right) \quad (6)$$

where σ_{BC} is the size of reception field, and $G(x,y; \sigma)$ is an expression of a two-dimensional Gaussian function.

1.1.3 Amacrine cells

In rod pathways, rod bipolar cells do not connect directly with ganglion cells but via amacrine cells and cone bipolar cells. Amacrine cells connect with cone bipolar cells by gap junction, making excitatory electrical synapses with ON bipolar cells and inhibitory synapses with OFF bipolar cells. Maximum and minimum filterings are used to simu-

late the excitation and inhibition of AII amacrine cells in ON and OFF channels, which are written as follows

$$I_{AC}^{on}(x,y) = \max_{z \in \Omega(x,y)} I_{BC}^{on}(z) \quad (7)$$

$$I_{AC}^{off}(x,y) = \min_{z \in \Omega(x,y)} I_{BC}^{off}(z) \quad (8)$$

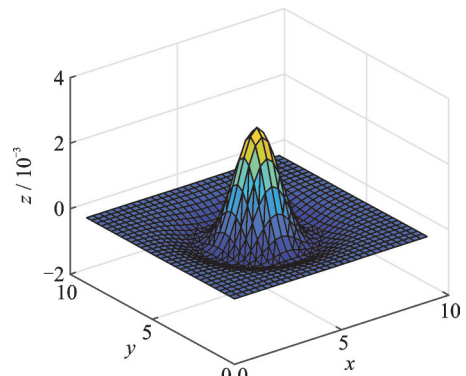
where $\Omega(x,y)$ is a local patch at center (x,y) .

1.1.4 Ganglion cells

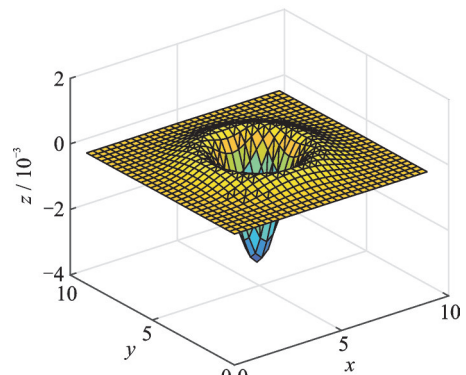
Ganglion cells on the one hand receive signals from bipolar cells originate in cones, as $I_{BC}^{\delta}(x,y)$, and originate in rod on the other, as $I_{AC}^{\delta}(x,y)$. According to previous research, the concentric circle structure and spatial characteristics of ganglion cell receptive field can be well simulated by difference of Gaussian (DoG) function^[15]

$$\text{DoG}(x,y) = A_{cen}G(x,y; \sigma_{cen}) - A_{sur}G(x,y; \sigma_{sur}) \quad (9)$$

where σ_{cen} and σ_{sur} denote the size of the center and surround structure in reception fields. A_{cen} and A_{sur} refer to the gain factor of two structures. The receptive fields of ganglion cells simulated by DoG function is shown in Fig.2. The ON-type and OFF-type reception fields are displayed in Figs.2(a) and (b),



(a) ON-type RF



(b) OFF-type RF

Fig.2 Schematic diagram of reception field simulated by DoG

respectively. The outputs of ON and OFF channels are calculated as follows

$$I_{BC-GC}^{\hat{o}}(x, y) = I_{BC}^{\hat{o}}(x, y) \times \text{DoG}(x, y) \quad (10)$$

$$I_{AC-GC}^{\hat{o}}(x, y) = I_{AC}^{\hat{o}}(x, y) \times \text{DoG}(x, y) \quad (11)$$

where $I_{BC-GC}^{\hat{o}}(x, y)$ and $I_{AC-GC}^{\hat{o}}(x, y)$ refers to the output originate in cones and rods, respectively.

1.2 Image dehazing

The formation of haze images can be explained by atmospheric scattering model, shown as

$$I(x, y) = J(x, y)t(x, y) + A(1 - t(x, y)) \quad (12)$$

where $I(x, y)$ and $J(x, y)$ denote the observed image and original image, A is the global atmospheric light and $t(x, y)$ the transmission of the reflected light. Considering the dark channel prior is invalid in sky region, the sky region is separated first in the proposed method, and the values of A and t are calculated based on the output of ON and OFF channels.

Obviously, sky region is characterized by high brightness, low saturation and low contrast. Correspond to above characteristics, the conditions for segmentation can be specifically described as follows

$$\begin{cases} I_{AC}^{\text{on}}(x, y) > l \\ I_{AC}^{\text{on}}(x, y) - I_{AC}^{\text{off}}(x, y) < s \\ I_{BC-GC}^{\text{off}}(x, y) + I_{AC-GC}^{\text{off}}(x, y) < c \end{cases} \quad (13)$$

where l , s and c denote the thresholds of brightness, saturation and contrast. A segmentation image $S(x, y)$ is obtained according to above conditions. After the sky region is segmented, the atmospheric light A can be easily estimated by ON channel. Concretely, we take the average of the maximum 5% value in $I_{AC}^{\text{on}}(x, y)$ belonging to the sky region as the estimated value of A , described as

$$A = \text{mean}(\max_{0.05} I_{AC}^{\text{on}}(x, y)) \quad (14)$$

According to the atmospheric scattering model and dark channel prior, the transmission t can be estimated by

$$t(x, y) = 1 - \min_{p \in \hat{\Omega}(x, y)} \left(\min_{c \in \{R, G, B\}} \frac{I^c(p)}{A^c} \right) \quad (15)$$

The second term of Eq.(15) is the dark channel of the normalized image $\frac{I^c(p)}{A^c}$. Considering the similarity of the OFF channel and dark channel im-

ages, we first use the output of the OFF channel to estimate t as follows

$$t^{\text{off}}(x, y) = 1 - \omega \frac{I_{AC}^{\text{off}}(x, y)}{A} \quad (16)$$

where ω is for keeping a small amount of haze to make image natural. To fix the halo effect, we define the transmission of the sky region as a constant value t^{sky} . The final transmission map is calculated by weighted sum of t^{sky} and $t^{\text{off}}(x, y)$. The weights are selected by the pixel value of $S_g(x, y)$, which is $S(x, y)$ after Gaussian filter, shown as

$$S_g(x, y) = S(x, y) \times G(x, y, \sigma_s) \quad (17)$$

$$t(x, y) = S_g(x, y)t^{\text{sky}} + (1 - S_g(x, y))t^{\text{off}}(x, y) \quad (18)$$

where σ_s is the size of Gaussian filter. At last, guided filtering is performed to refine the transmission map. The restored image is calculated by

$$J(x, y) = \frac{I(x, y) - A}{t(x, y)} + A \quad (19)$$

2 Eagle-Vision-Based Object Detection

Visual attention describes the process that the visual system will give priority to a specific area in the image and allocate more resources to it. The living and predation environments of eagles are complex and changeable. Mueller's research^[16] stated that the choice of targets during predation is not random, but shows more interest in special objects or regions than background. Dutta et al.^[17] made electrical stimulation experiments on barn owls, concluding that the barn owl's visual system has a pop-out mechanism, which can help them to locate targets accurately. Moreover, related research shows conspicuousness^[18], oddity^[19], color differences^[16] are typical factors that affect target selection in eagle's predatory behavior, and these characteristics are all related to visual attention. High density of cone cells in eagle's foveas makes them more sensitive to color and contrast features than other species. In this section, we proposed an object detection algorithm on the basis of eagle's visual attention mechanism. The intensity, color antagonism and contrast sensitivity of the images are calculated, and a spatial Gaussian pyramid is generated to simulate

the center-surround receptive field mechanism. Random Forest is used to further improve the performance of the algorithm and generate a saliency map.

Region with the highest saliency value in the map is regarded as the object. The illustration of the proposed method is shown in Fig.3.

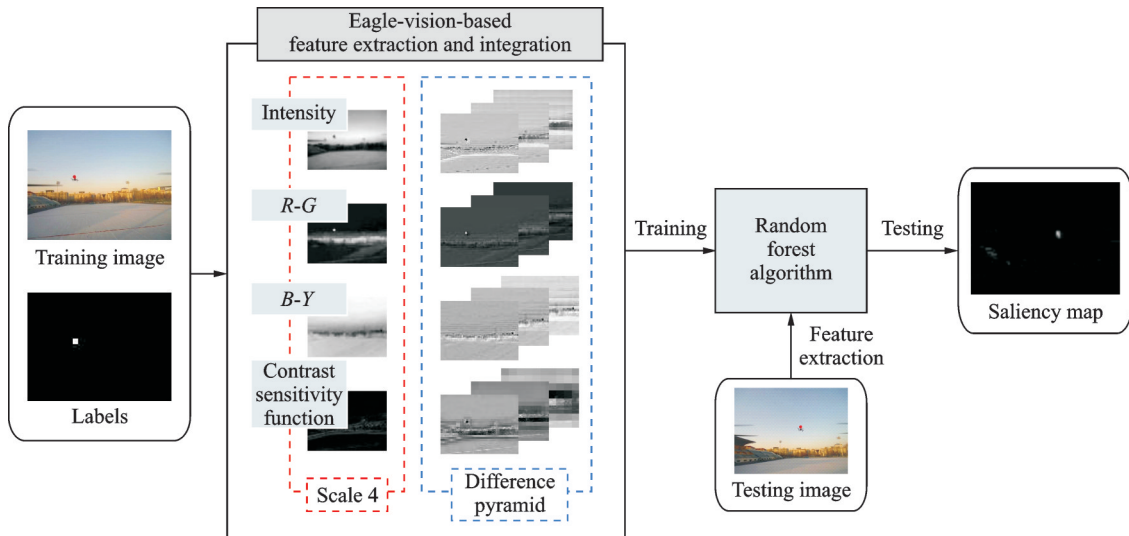


Fig.3 Schematic diagram of the proposed object detection method

2.1 Feature extraction

The cones in eagle's retina play an important role in color perception. Many studies confirmed that eagle has four types of single cone cells, which could sense four different frequency bands of light. In contrast of three ones in human, eagle may have an acute four-color vision^[20]. Color information is processed in an antagonistic manner in eagle's visual system. Four types of photoreceptors generate red-green and blue-yellow antagonistic signals, then transfer the signals along the tectofugal pathway. We calculate the primary features of the image based on the eagle's color antagonistic mechanism. Given an RGB input image, the intensity channel is defined as

$$I = \max\{R, G, B\} \quad (20)$$

Color antagonistic feature is calculated using four colors of red R , green G , blue B and yellow Y . The yellow channel of the RGB image, $Y = 0.5 \times (R + G)$, is synthesized by the red and green channels. Two color antagonistic channels are created: $RG = R - G$ for red-green antagonistic channel and $BY = B - Y$ for blue-yellow antagonistic channel.

Spatial contrast sensitivity is defined to describe the ability of distinguish adjacent areas with

contrast differences. The maximum value of the distinguishable frequency is defined as visual acuity, which can be obtained by anatomical or electrical behavior experiments. The former calculates the visual acuity by measuring the density of photoreceptors. Related results indicate that the visual acuity of wedge-tailed hawk is about 140 cpd (cycle per degree), and that of human is about 33–73 cpd^[21]. Results obtained by behavior experiments have similar results and concluded that eagle's visual acuity is much higher than other avians^[22]. The relationship between contrast sensitivity and visual acuity can be described by the contrast sensitivity function (CSF). Compared with other species, eagle's CSFs have narrower band-pass, showing a symmetrical inverted U-shaped trend. Their distributions focusing on high spatial frequencies reflected that eagles are sensitive to dim features. According to the sensitivity normalized data of eagle, the CSF can be well fitted by a double-exponential function^[3], which is computed as follows

$$\text{CSF}(x, y) = K_c E(x, y, \alpha_c) + K_s E(x, y, \alpha_s) \quad (21)$$

$$E(x, y, \alpha) = \exp(-\pi\alpha(x^2 + y^2)) \quad (22)$$

where K_c , K_s , α_c , α_s are fixed parameters. We applied CSF to calculate textures and local contrast features of image, and the contrast sensitivity chan-

nel is calculated as

$$C(x,y)=g(x,y)\times \text{CSF}(x,y) \quad (23)$$

where $g(x,y)$ is the grayscale of the input image.

2.2 Center-surround operation

Tectofugal pathway, composed of retina, optic tectum, nucleus and ectostriatum, is the most important pathway in eagle's visual system. Neurons in tectofugal pathway transmit visual information progressively, extracting and integrating primary visual features such as color, edges and textures. Reception field of optic nerve cells in tectofugal pathway has a center-surround structure, and stimuli presented in center regions are activated while visual neurons in surround regions are inhibited. Inspired by Itti's visual attention model^[23], a modified difference pyramid is used to simulate the operation of the central-surround structure. To avoid the loss of information caused by interpolations in Itti's model, we adopted a seven-layer pyramid. The center is the feature map at scale $s \in \{1, 2, 3\}$, and the corresponding surround is at scale $s + \gamma$, with $\gamma = 4$. A feature vector \bar{F} is calculated as follows

$$\bar{F} = F(s) \ominus F(s + \gamma) \quad (24)$$

where $F \in \{I, RG, BY, C\}$ represents the four types of features, and the operator \ominus represents the point-by-point subtraction after normalizing the size of feature maps at different scales. All feature maps are uniformly normalized to the size of scale 4. The feature map at scale 4 is not calculated with other layers but defined as the feature vector directly. Thus, we have a 16-dimension feature vector for a single RGB image.

2.3 Random Forest algorithm

Random Forest^[24] is a supervised ensemble learning algorithm that widely used in classification and regression tasks. On the basis of bagging, random attribute selection is implemented in the training of decision trees, which makes Random Forests have good accuracy, insensitivity to feature outliers, and strong ability to interfere. To enhance the performance of object detection in specific scenes, Random Forest is used to promote the synthesis of saliency maps. In this paper, object detection is re-

garded as a binary classification task. The procedure of proposed object detection algorithm is summarized as follows

Step 1 Annotate the training samples, the pixels in the target area are marked as 1, others are marked as 0.

Step 2 Extract the low-level features including intensity, color antagonism and contrast sensitivity, and obtain a 16-dimensional feature vector for each image.

Step 3 Train the Random Forest classifier with labeled images.

Step 4 Input the test images to the classifier, and generate a preliminary saliency map according to the confidence of predictions.

Step 5 Binarize the saliency map. The threshold b for binarization is set as

$$b = \sigma \cdot \max(M(x,y)) \quad (25)$$

where $M(x,y)$ is the pixel value of saliency map at (x,y) , and σ is fixed to 0.75 for separating the salient regions.

At last, the overall flow chart of the method is shown in Fig.4.

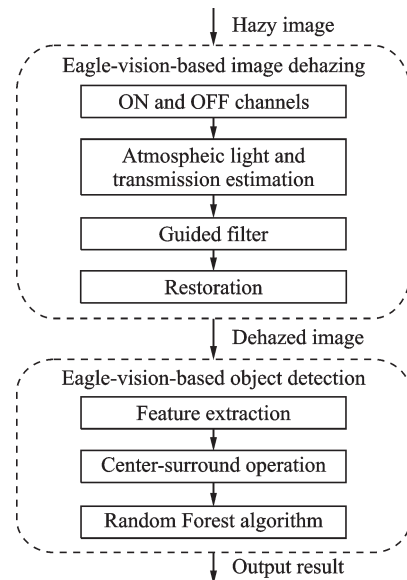


Fig.4 Overall flow chart of the method

3 Results and Analysis

Performances of the proposed dehazing and visual attention model are tested on two cases of im-

age sequences pictured in UAV formation scenarios. In the first experiment, we tested the effect of the dehazing method on both cases and compared it with He's algorithm^[10]. In the second experiment, we tested the object detection algorithm and compared it with the HC^[11], SR^[25], SO^[26] and GS^[27] methods. The details of two experiments are given as follows.

3.1 Image dehazing

The parameters used in this experiment are set as follows: $\alpha=7$, $\beta=-0.5$, $\sigma_{BC}=7$, $\sigma_{cen}=0.8$, $\sigma_{sur}=0.7$, $A_{cen}=A_{sur}=1$, $l=0.65$, $s=0.1$, $c=$

0.08 , $\omega=0.98$, $t^{sky}=0.65$, $\sigma_s=5$.

Fig.5 shows the processed results of two cases of experimental images using He's method and our method. As shown in Fig.5, He's method enhanced the image contrast remarkably, however, the color tone of the restored image shifts and loses the true color of the original appearance. The estimation of transmission is lower than the actual value, which leads to the severe halo effect occurring in the sky region. The halo effect makes UAV detection more challenging. By contrast, our result restores clear details of the scenarios with a natural color tone.

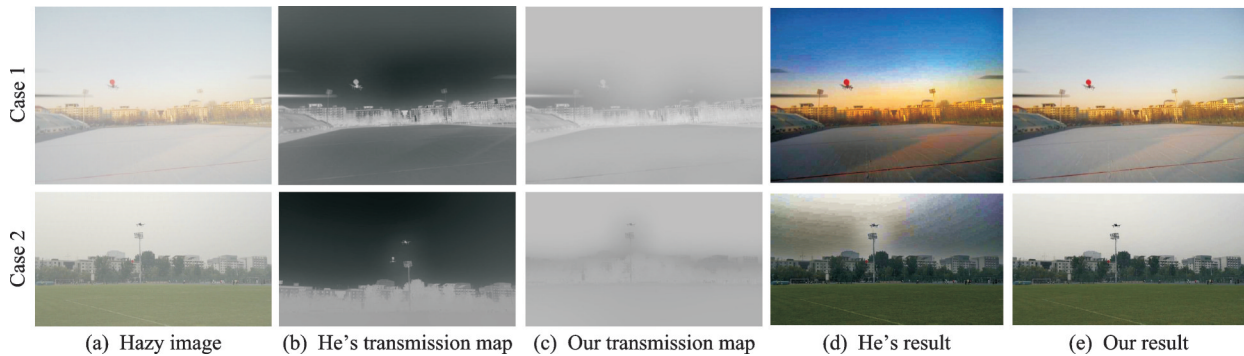


Fig.5 Results of image dehazing

3.2 Object detection

The parameters used in this experiment are set as follows: $K_c=0.2$, $K_s=0.3$, $\alpha_c=0.25$, $\alpha_s=0.32$.

In this experiment, Random Forest is trained with three images, and other images in the same scenario are used for testing. Fig.6(a) is the de-

hazed image processed by eagle-vision-based dehazing method, Figs.6(b)—(f) exhibit the saliency maps generated by SR, HC, SO, GS and the proposed methods, and Fig.6(g) is the binarized saliency map of Fig.6(f). Results above show that all UAVs are highlighted and backgrounds are sup-

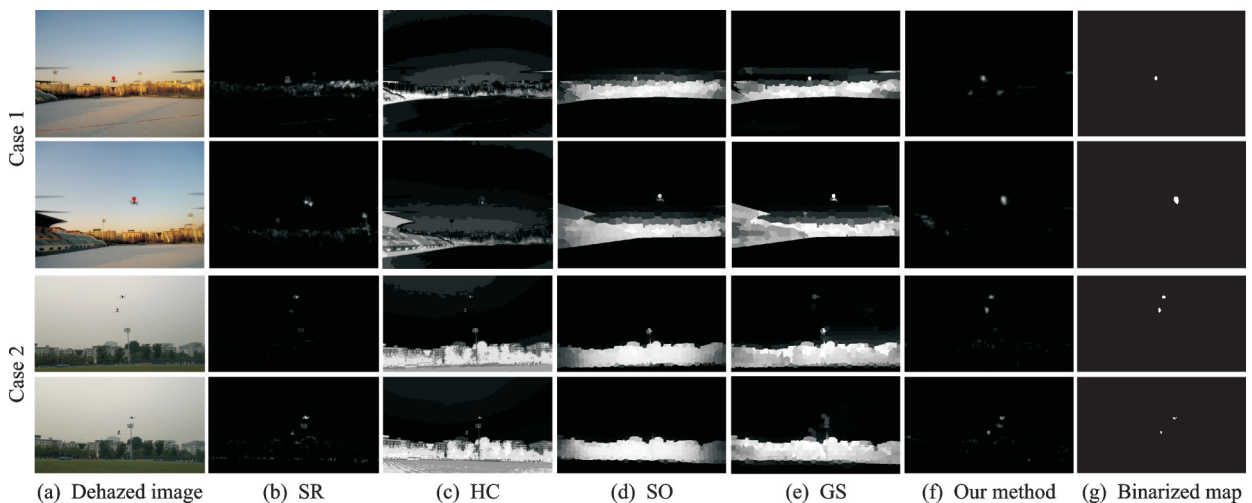


Fig.6 Results of object detection

pressed by the proposed method. In comparison, object detected by SR is not complete. In the saliency maps of HC, SO and GS, the background of the test image is not well suppressed.

Fig.7 shows the testing results on a more challenging task. Fig.7(a) is the hazy image, Figs.7(b) — (e) present the saliency maps generated by SR, HC, SO and the proposed method, Fig.7(f) is the binarized saliency map of Fig.7(e), Fig.7(g) shows the detection result with bounding boxes, and Figs.7(h) are the enlarged views of Figs.7(a)

and (g), showing the details of target area. As shown in Figs.7(a) and (h), the UAV with a red drogue overlaps with building in background which makes it hard to detect. Through the comparison of saliency maps, it is found that pixels in saliency map generated by the proposed method have higher values in the area of both two targets. However, in the saliency map generated by SR, the UAV with a red drogue was not determined to be a salient object, and pixels belonging to the background reach high value in HC's and SO's results. Thus, our method is more accurate and reliable than the other three methods.

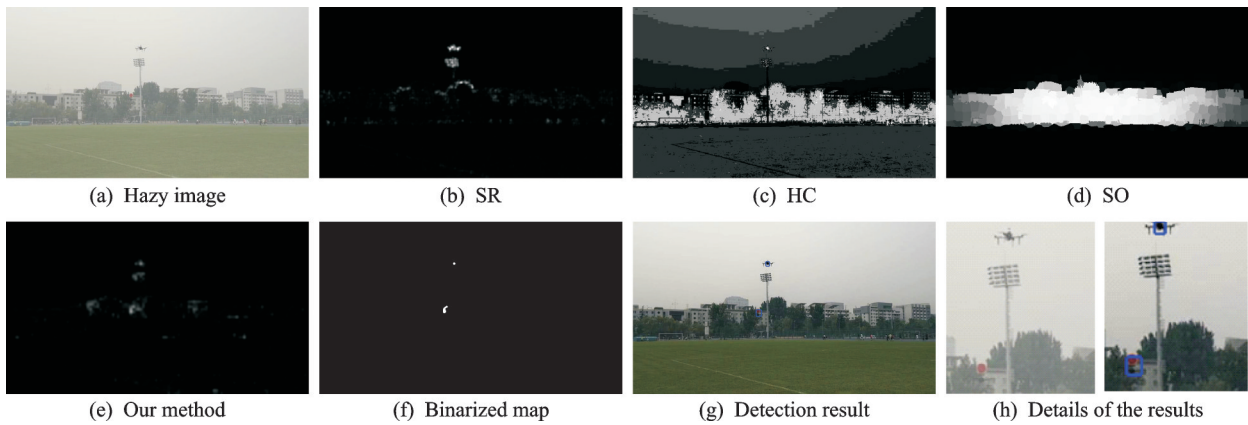


Fig.7 Detection results in challenging task

Fig.8(a) shows the saliency map of hazy image. Detection results of the proposed method on hazy and dehazed images are presented in Fig.8(b) and Fig.8(c). In the saliency map of dehazed image (Fig.6(f)), the saliency value of the object area is significantly higher than that of the background area, and all the objects are detected accurately and

marked by bounding boxes. Without dehazing, the features and details of the images are not recovered. The saliency of objects is decreased, and an UAV is failed to detected in Case 2. Since the threshold of saliency map binarization is proportional to the maximum pixel value of the map and the difference of saliency value between objects and background is

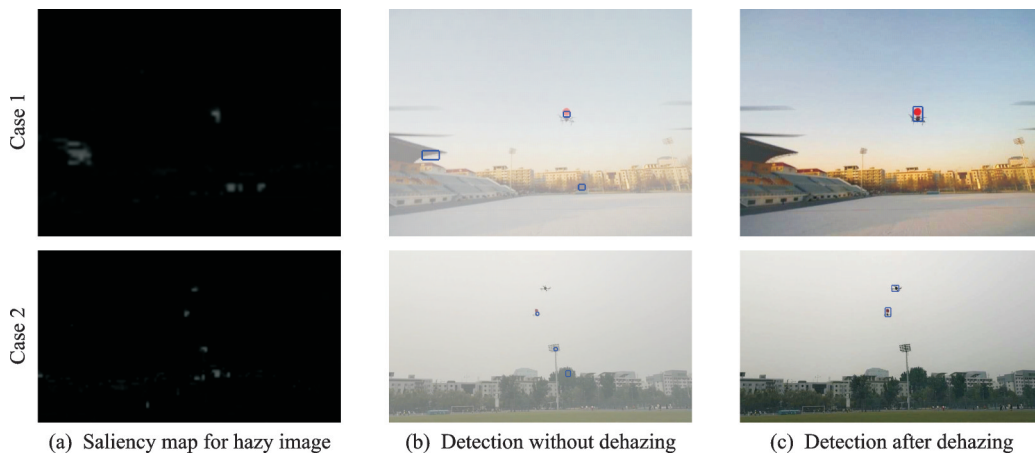


Fig.8 Detection results on hazy and dehazed images

smaller, object detection is more susceptible to background interference. Therefore, the precision is lower due to the false positives in background, and dehazing method plays a certain role in detection under severe weather condition.

Fig. 9 shows the continuous detection error of the image sequence in Case 1. The resolution of images in Case 1 is 640 pixel \times 480 pixel. UAVs in the 30 continuous images are labeled manually. The detection error is defined as the distance between the center coordinates of the bounding box in labeled image and saliency map. Results verify that the proposed method has the smallest detection error among the five methods.

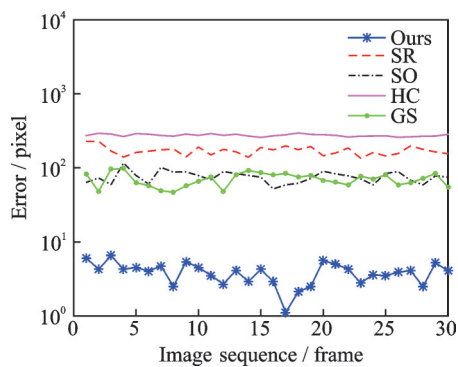


Fig.9 Detection error

4 Conclusions

In this paper, an eagle-vision-based object detection method for UAV formation in hazy weather is proposed. Inspired by the signal processing mechanism of ON and OFF channels in eagle's retina, the values of atmospheric light and transmission are estimated to restore the hazy image. An object detection method on the basis of eagle's visual attention mechanism is presented. Performances of the proposed algorithm are tested and compared on two cases of images pictured in UAV formation scenarios. Experimental results verify that the proposed method has superior performance over traditional methods. Moreover, the proposed method is robust and reliable in challenging environments, which could provide guarantees for UAV formation.

References

- [1] CHENG M M, MITRA N J, HUANG X, et al. Global contrast based salient region detection[J]. IEEE Transactions on Pattern Analysis and Machine Intelligence, 2015, 37(3): 569-582.
- [2] HE K M, GKIOXARI G, DOLLAR P, et al. Mask R-CNN[C]//Proceedings of 2017 IEEE International Conference on Computer Vision. Venice, Italy: IEEE, 2017: 2961-2969.
- [3] DENG Y M, DUAN H B. Avian contrast sensitivity inspired contour detector for unmanned aerial vehicle landing[J]. Science China Technological Sciences, 2017, 60(12): 1958-1965.
- [4] WANG X H, DUAN H B. Hierarchical visual attention model for saliency detection inspired by avian visual pathways[J]. IEEE/CAA Journal of Automatica Sinica, 2019, 6(2): 540-552.
- [5] SUN Y B, DENG Y M, DUAN H B, et al. Bionic visual close-range navigation control system for the docking stage of probe-and-drogue autonomous aerial refueling[J]. Aerospace Science and Technology, 2019, 91: 136-149.
- [6] DUAN H B, XIN L, CHEN S J. Robust cooperative target detection for a vision-based UAVs autonomous aerial refueling platform via the contrast sensitivity mechanism of eagle's eye[J]. IEEE Aerospace and Electronic Systems Magazine, 2019, 34(3): 18-30.
- [7] DUAN H B, XIN L, XU Y, et al. Eagle-vision-inspired visual measurement algorithm for UAV's autonomous landing[J]. International Journal of Robotics and Automation, 2020, 35(2): 94-100.
- [8] DENG Y M, DUAN H B. Biological eagle-eye-based visual platform for target detection[J]. IEEE Transactions on Aerospace and Electronic Systems, 2018, 54(6): 3125-3136.
- [9] DUAN H B, DENG Y M, WANG X H, et al. Biological eagle-eye-based visual imaging guidance simulation platform for unmanned flying vehicles[J]. IEEE Aerospace and Electronic Systems Magazine, 2013, 28(12): 36-45.
- [10] HE K M, SUN J, TANG X O. Single image haze removal using dark channel prior[J]. IEEE Transactions on Pattern Analysis and Machine Intelligence, 2011, 33(12): 2341-2353.
- [11] BERMAN D, TREIBITZ T, AVIDAN S. Non-local image dehazing[C]//Proceedings of 2016 IEEE Conference on Computer Vision and Pattern Recogni-

- tion. Piscataway, USA: IEEE, 2016: 1674-1682.
- [12] JONES M P, PIERCE K E, WARD D. Avian vision: A review of form and function with special consideration to birds of prey[J]. *Journal of Exotic Pet Medicine*, 2007, 16(2): 69-87.
- [13] SCHILLER P H. Parallel information processing channels created in the retina[J]. *Proceedings of the National Academy of Sciences*, 2010, 107(40): 17087-17094.
- [14] BLOOMFIELD S A, VOLGYI B. The diverse functional roles and regulation of neuronal gap junctions in the retina[J]. *Nature Reviews Neuroscience*, 2009, 10(7): 495-506.
- [15] RODIECK R W, STONE J. Analysis of receptive fields of cat retinal ganglion cells[J]. *Journal of Neurophysiology*, 1965, 28(5): 832-849.
- [16] MUELLER H C. Factors influencing prey selection in the American kestrel[J]. *The Auk*, 1974, 91(4): 705-721.
- [17] DUTTA A, WAGNER H, GUTFREUND Y. Responses to pop-out stimuli in the barn owl's optic tectum can emerge through stimulus-specific Adaptation[J]. *Journal of Neuroscience*, 2016, 36(17): 4876-4887.
- [18] HUNT K A, BIRD D M, MINEAU P, et al. Selective predation of organophosphate-exposed prey by American kestrels[J]. *Animal Behaviour*, 1992, 43(6): 971-976.
- [19] MULLER H C. Oddity and specific searching image more important than conspicuousness in prey selection[J]. *Nature*, 1971, 233: 345-346.
- [20] CHEN D M, COLLINS J S, GOLDSMITH T H. The ultraviolet receptor of bird retinas[J]. *Science*, 1984, 225: 337-340.
- [21] REYMOND L. Spatial visual acuity of the eagle *aquila audax*: A behavioural, optical and anatomical investigation[J]. *Vision Research*, 1985, 25(10): 1477-1491.
- [22] HARMENING W M, NIKOLAY P, ORLOWSKI J, et al. Spatial contrast sensitivity and grating acuity of barn owls[J]. *Journal of Vision*, 2009, 9(7): 1-12.
- [23] ITTI L, KOCH C, NIEBUR E. A model of saliency-based visual attention for rapid scene analysis[J]. *IEEE Transactions on Pattern Analysis and Machine Intelligence*, 1998, 20(11): 1254-1259.
- [24] BREIMAN L. Random forests[J]. *Machine Learning*, 2001, 45(1): 5-32.
- [25] HOU X D, ZHANG L Q. Saliency detection: A spectral residual approach[C]//*Proceedings of 2007 IEEE Conference on Computer Vision and Pattern Recognition*. Minneapolis, USA: IEEE, 2007: 1-8.
- [26] ZHU W J, LIANG S, WEI Y C, et al. Saliency optimization from robust background detection[C]//*Proceedings of 2014 IEEE Conference on Computer Vision and Pattern Recognition*. Columbus, USA: IEEE, 2014: 2814-2821.
- [27] WEI Y C, WEN F, ZHU W J, et al. Geodesic Saliency Using Background Priors[C]//*Proceedings of 2012 European Conference on Computer Vision*. Florence, Italy: IEEE, 2012: 29-42.

Acknowledgements This work was partially supported by the Science and Technology Innovation 2030-Key Projects (Nos. 2018AAA0102303, 2018AAA0102403); the Aeronautical Science Foundation of China (No. 20175851033); and the National Natural Science Foundation of China (Nos. U1913602, U19B2033, 91648205, 61803011).

Authors Ms. LI Hao received her B.S. degree in Control Theory and Engineering from Beihang University (BUAA), Beijing, China, in 2017. She is currently pursuing the Master degree in Control Engineering at the School of Automation Science and Electrical Engineering, Beihang University. Her current research interest includes bio-inspired computation and computer vision.

Dr. DENG Yimin is currently an assistant professor of School of Automation Science and Electrical Engineering, Beihang University (BUAA), Beijing, China. He received the Ph.D. degree from Beihang University in 2017. His current research interests include bio-inspired computation, advanced flight control, and biological computer vision.

Author contributions Ms. LI Hao designed the study, completed the experiments and wrote the manuscript. Dr. DENG Yimin conducted the analysis and contributed to the critical advices. Mr. XU Xiaobin participated in the experiments and analysis. Mr. SUN Yongbin participated in the experiments and discussion. Dr. WEI Chen contributed to the discussion and background of the study. All authors commented on the manuscript draft and approved the submission.

Competing interests The authors declare no competing interests.

一种基于鹰视觉的雾霾天气无人机编队目标检测方法

李 皓, 邓亦敏, 徐小斌, 孙永斌, 魏 晨

(北京航空航天大学自动化科学与电气工程学院, 北京 100083, 中国)

摘要: 本文提出了一种仿鹰眼视觉特性的雾霾天气下无人机编队目标检测算法。通过模拟鹰视网膜中 ON 和 OFF 通路的视觉信号处理机制, 对大气光与透射率的值进行估计从而复原雾霾图像。同时利用鹰视觉系统的颜色拮抗机制与对比度敏感函数提取除雾图像下的目标特征, 模拟中央-周边结构感受野特性对特征进行整合, 最后通过随机森林算法生成目标显著图以进行目标检测。实验结果表明本文提出的算法能够有效检测出雾霾天气下无人机编队场景中的无人机目标, 与其他传统方法相比, 本文算法具有更好的检测效果。

关键词: 目标检测; 鹰视觉系统; 无人机编队; 图像去雾